



Physical properties of chemical vapour deposited nanostructured carbon thin films

D.B. Mahadik, S.S. Shinde, C.H. Bhosale, K.Y. Rajpure*

Electrochemical Materials Laboratory, Department of Physics, Shivaji University, Kolhapur, Maharashtra 416004, India

ARTICLE INFO

Article history:

Received 17 September 2010

Received in revised form 31 October 2010

Accepted 2 November 2010

Available online 10 November 2010

Keywords:

Carbon films

Chemical vapour deposition

XRD

SEM

Contact angle

FTIR

Raman

ABSTRACT

A simple thermal chemical vapour deposition technique is employed for the deposition of carbon films by pyrolysing the natural precursor “turpentine oil” on to the stainless steel (SS) and FTO coated quartz substrates at higher temperatures (700–1100 °C). In this work, we have studied the influence of substrate and deposition temperature on the evolution of structural and morphological properties of nanostructured carbon films. The films were characterized by using X-ray diffraction (XRD), scanning electron microscopy (SEM), contact angle measurements, Fourier transform infrared (FTIR) and Raman spectroscopy techniques. XRD study reveals that the films are polycrystalline exhibiting hexagonal and face-centered cubic structures on SS and FTO coated glass substrates respectively. SEM images show the porous and agglomerated surface of the films. Deposited carbon films show the hydrophobic nature. FTIR study displays C–H and O–H stretching vibration modes in the films. Raman analysis shows that, high ID/IG for FTO substrate confirms the dominance of sp^3 bonds with diamond phase and less for SS shows graphitization effect with dominant sp^2 bonds. It reveals the difference in local microstructure of carbon deposits leading to variation in contact angle and hardness, which is ascribed to difference in the packing density of carbon films, as observed also by Raman.

© 2010 Elsevier B.V. All rights reserved.

1. Introduction

Carbon is one of the most abundant elements in the universe and the most versatile material existing amorphous, glassy and crystalline forms. This element is the basis of life on Earth and constitutes interiors of the celestial objects: outer planets, Uranus, Neptune, and white dwarf stars. Carbon is often considered to be silicon of the future because of the unique properties resulting from the variety of possible structural forms. Owing to their unique atomic structure, outstanding mechanical strength, thermal conductivity and versatile electronic properties, carbon nanotubes (CNTs) are key components of a wide range of scientific and technological studies. In recent years, many efforts have led to the development of versatile chemical modification methodologies, targeting CNT derivatives with even more attractive features. A wide range of electronic properties of carbon from insulating/semiconducting diamond to metal-like graphite, nanotubes, and graphene sheets yields many novel technological applications such as electron field emitters for optical displays [1,2], micro-fabricated X-ray sources [3], electrode material for fuel cells [4,5], Lithium ion batteries [6], support for catalyst [7–9], tips for scanning probe microscopy [10], electrochemical actuators [11], sensors

[12], nano-biotechnology [13], etc. Such versatility of this element in nature results from the unique property of a carbon atom to form bonds of many different configurations, called hybridizations: linear sp^1 , planar sp^2 , tetrahedral sp^3 , etc. All of these cause great scientific interest in thermodynamic properties of carbon. In addition to initially developed laser furnace [14] and arc discharge [15] techniques, catalytic chemical vapour deposition (CCVD) method [16,17] has been contrived for large scale production of carbon nanotubes, with various carbon source molecules tested such as carbon monoxide, methane, benzene, xylene, toluene, etc. These carbon sources are related to fossil fuels which may not be sufficient in near future; so researchers switched over to reproducible natural carbon source like camphor and grown various kinds of nano-carbons [18,19]. This gives new idea to develop nanotechnology with eco-friendly and environmentally clean carbon source: turpentine oil, which is derived from the oleoresin of Pinus species particularly from *Pinus palustris* of Pinaceae family. Our effort is mainly focused on identifying and using regenerative, reproducible source. A simple template synthesis method has been explored [20,21] for preparing micro and nanostructured materials. In the present paper, nanostructured carbon films are grown using a natural precursor “turpentine oil ($C_{10}H_{16}$)” as a carbon source in the simple thermal chemical vapour deposition method, unlike PECVD, MPCVD, PLD, etc., that are commonly used for the deposition of various types of carbon films. It is worth noting that for deposition on complex geometrical structures and large sized sub-

* Corresponding author. Tel.: +91 231 2609435; fax: +91 231 2691533.

E-mail address: rajpure@yahoo.com (K.Y. Rajpure).

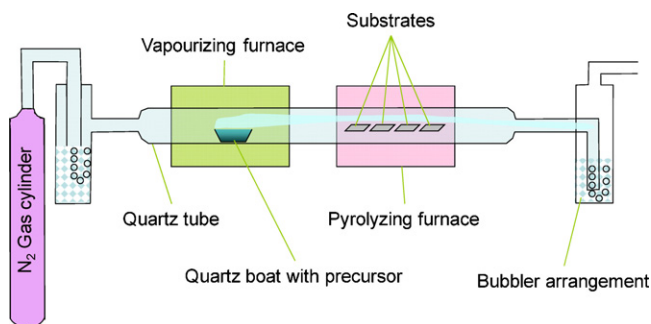


Fig. 1. Schematic diagram of the chemical vapour deposition system used in the present experiments.

strate, thermal CVD is an ideal choice. In the preparation of carbon films, high percentage of sp^3 bonded carbon atoms is preferred in crystal lattice. The influence of substrate surface topography (viz. stainless steel, fluorine doped tin oxide coated quartz) and temperature on the evolution of carbon allotropes surfaces topography/microstructural and structural properties are investigated and discussed. The ratio of intensities of D and G bands (ID/IG) of nanostructured carbon films is studied using Raman spectroscopy.

2. Experimental

The carbon films were deposited on to the stainless steel (SS) and fluorine doped tin oxide (FTO) coated quartz glass substrates using thermal chemical vapour deposition (CVD) technique. The deposition unit contains a 1.5 meter long quartz tube (diameter 25 mm) serves as a thermal CVD reactor kept horizontally inside two horizontal furnaces along the axis of both of them. Schematic diagram of the experimental set-up is shown in Fig. 1. The vapourizing furnace was used to vapourize turpentine oil ($C_{10}H_{16}$) and pyrolyzing furnace was used to pyrolyse the vapours of turpentine oil. In the quartz tube, stainless steel and FTO substrates (over which turpentine oil is to be pyrolysed and deposited) were placed in furnace. Prior to deposition, the whole deposition chamber was purged with nitrogen for 30 min. Then temperature of the pyrolyzing furnace was elevated from room temperature to desired deposition temperature under nitrogen atmosphere. Once, the substrates reached for desired temperature, turpentine oil (2 cm^3) kept in quartz boat was vapourized at 250°C and the vapourized gas was allowed to pass inside the quartz tube. The depositions were carried out in separate sets of experiments, for substrate temperatures as 800, 900, 1000 and 1100°C for 30 min. Nitrogen gas was flushed until the furnaces were cooled down to room temperature.

The structural characterization of deposited films was carried out, by analyzing the X-ray diffraction patterns obtained using $\text{CuK}\alpha$ ($\lambda = 1.5406\text{ \AA}$) radiation from a Philips X-ray diffractometer model PW-3710 within the span of angle $10\text{--}100^\circ$. The surface morphology was studied by using JEOL JSM-6360 scanning electron microscope (SEM), Japan. The wettability of the films was characterized by the measurement of static contact angle against water in air by contact angle meter (rame-hart Instrument Co., USA) at room temperature. The diameter of water droplet used for the measurements was 2.4 mm. Contact angles were measured at four different points for each sample, and the average value was adopted as the contact angle. FTIR spectra were recorded on a PerkinElmer spectrum-1 spectrophotometer. Raman-scattering experiments were performed in air at room temperature

with polarization incident light using a MultiRam (Bruker Made, Germany) spectrometer. The films were excited with 1064 nm line of Nd:YAG laser. The scattered light from the sample was passed through a broadband polarization scrambler to eliminate polarization effects in the monochromator. The scattered light was analyzed by means of a MultiRam spectrometer equipped with a LN₂-cooled Germanium (Ge) detector with quartz filter.

3. Results and discussion

3.1. X-ray diffraction

Fig. 2(a and b) shows the XRD patterns of carbon thin films grown on two kinds of substrates (a) stainless steel, (b) FTO coated quartz glass substrate at typical temperature 1000°C . These patterns are analyzed by using JCPDS cards no. 00-002-0456 (hexagonal) and 85-1799 (cubic: face-centered) respectively for SS and FTO substrates. The films are polycrystalline and fit well with the hexagonal (space group P63mc) and cubic: face-centered (space group Fm3m (225)) crystal structures for stainless steel and FTO coated substrates respectively. Films grown on SS and FTO show the formation of graphite and C60 carbon form respectively. The characteristic peaks appearing at $2\theta = 26.39^\circ$, 44.60° , and 74.29° displays the presence of graphitic carbon nanofibers [22] on SS substrate and peaks appeared at 30.89° , 32.51° , 46.30° , 48.30° , and 54.60° show the presence of C60 carbon nanostructure. Carbon film deposited on SS substrate shows the stronger (002) and (101) reflections and existence of some weak reflections viz. (102), (104) and (200). X-ray diffraction of carbon film deposited on FTO substrate illustrates stronger (511) and (822) reflections and some weak reflections such as (422), (531), (442), (620), (640), (642), (862), (1022), (864), (1133), (1222) and (1082). The reason for relatively lower peak intensities is the lower film thickness ($\sim 340\text{ nm}$) and scattering losses. The main driving force for the formation of graphite and C60 carbon is the thermal energy to activate the large interdiffusion between carbon and substrates.

3.2. Surface morphological study

Fig. 3(a–e) shows the SEM images of carbon thin films grown on to different substrates at 900 and 1000°C vapourizing furnace temperatures. The carbon films deposited on rough surfaces, at first, the atoms are accumulated in the holes that are existent on the surface substrate, but they cannot fill all the holes on the surface, in this situation the roughness is larger for smaller deposition time. As the time progresses, the atoms fill the holes and accumulate in surface and the roughness decreases. This effect promotes the reduction of surface energy and is related to the film growth rate. A smaller surface energy on the substrate is related to smoothing effect in the film deposition, and in this condition, the roughness

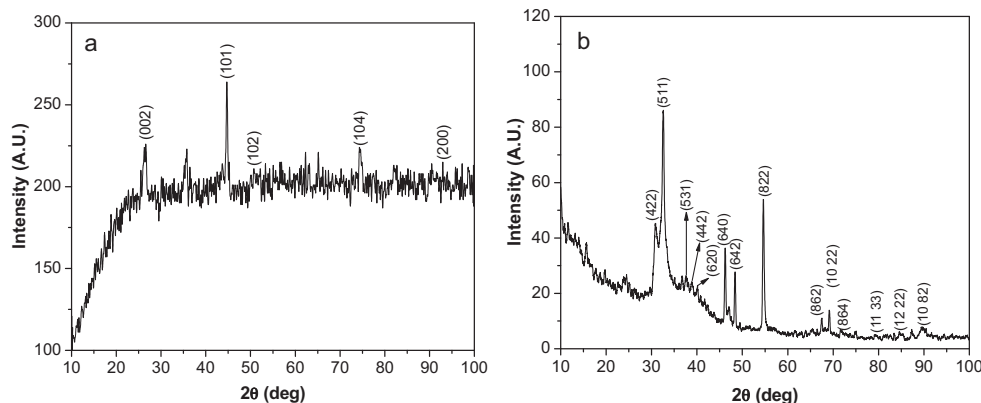


Fig. 2. XRD patterns of carbon thin films deposited onto the (a) SS and (b) FTO coated quartz glass substrates at 1000°C .

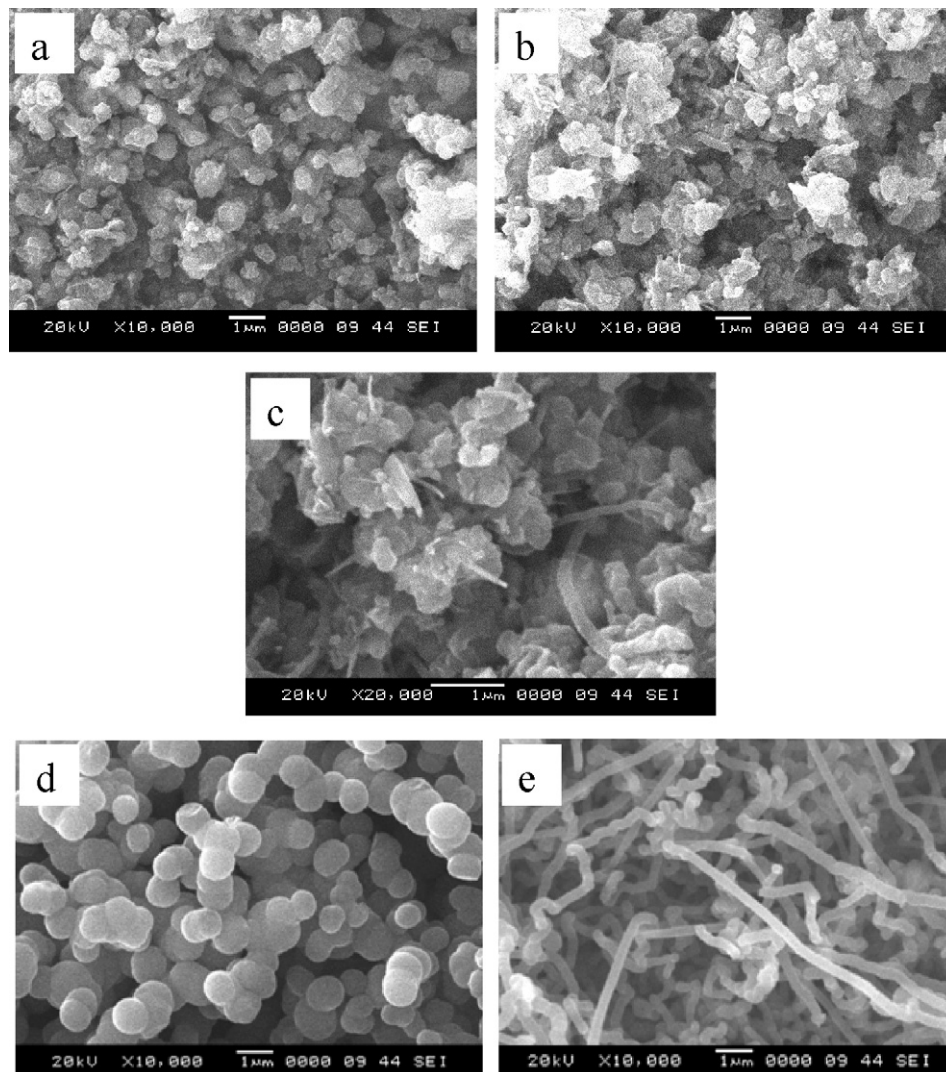


Fig. 3. SEM images of carbon thin films deposited on SS: (a) 900 °C, (b) 1000 °C and (c) 1000 °C (magnification 20,000×); FTO coated quartz glass substrate (d) 900 °C and (e) 1000 °C.

is smaller, because the atoms have more easiness to form the carbon films. If the surface energy is high, the roughness increases, because the atoms need high energy to league and to form the film. In this situation, the final roughness of the carbon films is strongly related to the surface energy [23]. The films deposited at 900 °C on SS substrate shows the existence of randomly dispersed but homogeneous agglomerates which appear to be loose felt. The deposited films are porous, scraggy but not fragile including voids. Further observation of the agglomerate surface shows that few nanofibers are physically entangled and loosely associated into agglomerates for 1000 °C as seen in Fig. 3(b and c). The nanofibers are not coiled but generally curved with an average outer diameter of 80–100 nm. The lengths of the nanofibers are difficult to determine definitely due to the entangled arrangement, but are at least of the order of microns. Agglomeration of grains is increased with increase in grain size at higher temperature. Fig. 3(d and e) shows the SEM pictures of the carbon films deposited on FTO glass substrate at 900 and 1000 °C. It clearly shows the dense and homogeneous network of beads and non-aligned CNTs. Highly dense, twisted and homogeneous nanobeads having average diameter of about 600 nm are observed at 900 °C. As we increase the temperature up to 1000 °C, the transformation of nanobeads into nanofibers is observed. From the images, it is seen that the uniformly distributed nanofibers are grown on the FTO glass than SS substrates. This could be related to

the lattice structure and defects on the substrate surface responsible for the chemical adsorption and subsequent nucleation and growth [24]. The bare glass substrate which belongs to the amorphous structure has smoother surface and less defects than the SS substrates. It illustrates that the lattice mismatch and defects on the surface affect the morphology as well as crystal orientation of resultant films. In these samples, the final film structure and morphology strongly depends on substrate surface conditions.

3.3. Contact angle measurement

Wettability of the film surface is evaluated by measuring static contact angles for water. The change in water contact angle values as a function of surface topography is shown in Fig. 4(a and b). All films show the hydrophobic behaviour. The contact angles of water droplets on the stainless steel and FTO coated surfaces are 134° and 114° respectively. The wettability of the film surface is mainly influenced by the surface chemical composition and morphology. The compact microstructure of the film surface shows higher water contact angle values as compared to smooth one. The reason for this behaviour may be that for high roughness gas bubbles are embedded between the water drop and the insulator surface [25]. The decrease of the contact angle relates to an increase in the hydrophilic nature due to the presence of oxidized films. This

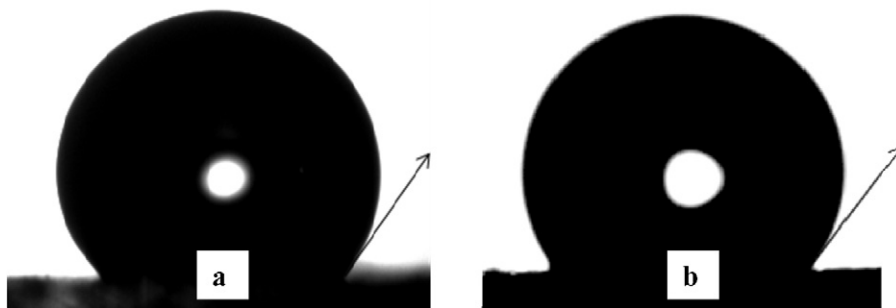


Fig. 4. Contact angle images of carbon films grown at 1000 °C on (a) SS and (b) FTO coated quartz glass substrates.

result is relevant to current interest in the application of carbon coatings as bioactive surfaces, for example, in tissue engineering scaffolds.

3.4. Infrared studies

FTIR spectra of carbon films deposited on to SS and FTO substrates are shown in Fig. 5(a and b) in order to decide the vibration modes for this material. The films show major peaks of O–H and C–H stretching, C–H–C bending and C=C. Films grown on SS substrate (Fig. 5(a)) show the strong IR peak of C–H bending vibration at 1020 and 1103 cm^{-1} due to the symmetric and antisymmetric stretching vibrations. The IR peaks at 3386 and 1621 cm^{-1} is associated with the adsorption of H_2O molecules and graphitic nature (C=C) of the carbon. The observed peak at 3386 cm^{-1} is corresponding to the stretching vibrations of O–H groups. The C–H stretching vibration peaks are observed at 2858 and 2930 cm^{-1} corresponding to sp^3 and sp^2 carbon atoms respectively. These are in good agreement with those reported by others [26], where the absorption for C–H stretching vibrations is found in the 2920–3060 cm^{-1} range on sp^2 bonded carbons and in the 2850–2920 cm^{-1} range on sp^3 bonded carbons. Additionally the H–C–H bending vibration is observed at 1460 cm^{-1} . Fig. 5(b) shows the FTIR spectra of carbon film deposited on FTO coated substrate, which reveals the stretching and bending vibrations of C–H groups, which are pertained to the residual FTO surface, with strong peaks appearing at 2951, 2917, 2850 and 1098 cm^{-1} . Further, the FTO cations are almost decomposed and eliminated after the thermal CVD process which is consistent with the intercalation and adsorption into the layers. The observed peaks of 3400 and 3500 cm^{-1} are corresponding to the stretching vibrations of O–H groups. The C=C and H–C–H vibrations are also observed at 1617 and 1098 cm^{-1} . In addition to that, Si–O bending vibration is seen at 512 cm^{-1} due to quartz glass.

3.5. Raman analysis

Raman spectroscopy is a fast and non-destructive tool for the effective analysis of bonding behaviour, domain size, internal stress, etc., in carbon thin films [27]. The Raman peak shapes, positions, shifts, half-width and intensity gives the comprehensive information about the chemistry and structure of carbon films. Inelastic, incoherent Stokes Raman scattering of light from the lattice of diamond was first observed by Ramaswamy [28] and investigated in detail by Solin and Ramdas [29]. The 1st order zone center sharp Raman peak of diamond and graphite is observed at 1333 and 1580 cm^{-1} respectively. All other types of carbon show broad peaks between 1100 and 1600 cm^{-1} [30]. Fig. 6(a and b) shows typical Raman spectra of carbon films grown at 1000 °C temperature onto the SS and FTO conducting quartz glass substrate respectively recorded in the region of 800–1800 cm^{-1} . The central peak of the crystalline C–C bonding in the longitudinal optical mode (LO mode) appears around 950–990 cm^{-1} is superimposed to the asymmetrical band [31], as observed in both the films. Two first order broad bands observed at ~1312, 1278 and 1542, 1534 cm^{-1} are named D-band (disorder/defect band) and G-band (graphitic band or E_{2g_2} mode), for SS and FTO glass substrate respectively. Interestingly, in most cases the intensity of the D-band is higher than the G-band in glassy carbon [32]. The prominent broad peak that observed in the grain boundaries at 1542–1544 cm^{-1} can be attributed to sp^2 -bonded carbon and the disordered allowed zone edge mode of graphite [33]. A careful observation of the intensities of G and D peaks in both cases indicates that CNTs deposited on SS substrate are expected to have a better graphitization compared to those deposited on FTO conducting glass substrate may be due to disorderliness in the film. The disorderliness in the carbon films originated from crystalline disordered graphite due to intermingling of s-(sp^3 -like) domains in the clusters of p-(sp^2 -like) graphite. For these samples, when the surface topography changes,

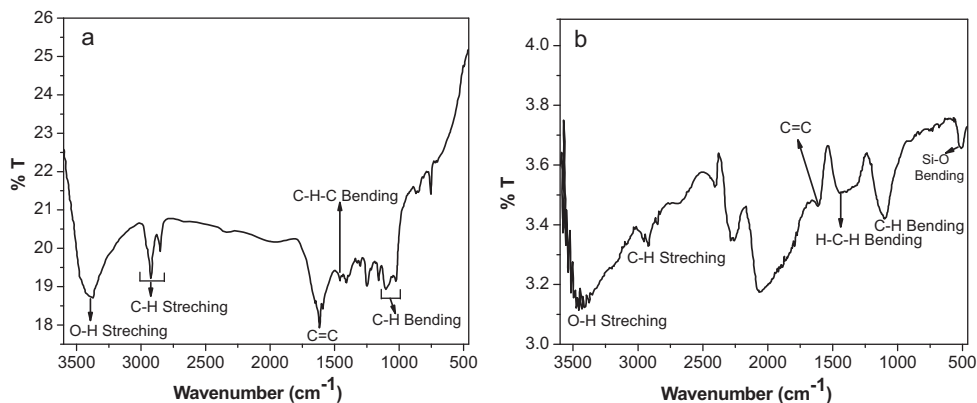


Fig. 5. FTIR spectra of carbon thin films deposited at 1000 °C onto the (a) SS and (b) FTO coated quartz glass substrates.

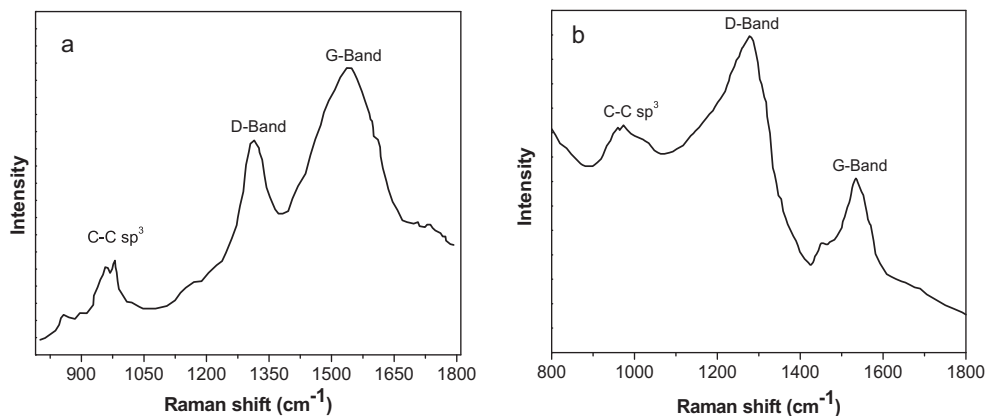


Fig. 6. Raman spectrum of carbon thin films deposited at 1000 °C onto the (a) SS and (b) FTO coated quartz glass substrates.

the change in the ID/IG occurs. The ID/IG is related to the increase in sp^3 bonds in the films. This effect can be confirmed with the presence of a small peak around 950–1000 cm^{-1} , this is related to the formation of sp^3 bonds due to the presence of C–C sp^3 bonds. We observed that the D band appeared at 1312 and 1278 cm^{-1} for SS and FTO substrates respectively. The intensity for all bands in the Raman spectra depends on surface topography. The sp^3 bonds are strong in the FTO than SS surface. These effects are related to the second order bands due to the presence of nanostructures in the films and surface energy generated by the different surface topography used. The surface energy of SS is high, due to the presence of the privileged points of deposition and this promotes the sp^2 bonds formation revealed from contact angle measurements. We noticed that decrease in ID/IG means increase of sp^2 bonds in the films, are promoted by the presence of graphitic form in the film consistent with the X-ray results. One of the characteristics of the graphite grains is the formation of bidimensional structures that privileged sp^2 bonds. The presence of second-order bands can influence these results, because these bands are related to different nanostructures formed during the growth of films, which are related to the surface topography.

3.6. Thermal conductivity and specific heat

It is essential to understand the thermo-physical properties of the carbon films, when working on those industrial and scientific applications that involve not only equipment design but also analysis, modeling and process control, where there are temperature-dependent physical, chemical and biochemical changes. Thermal conductivity analysis is done with the help of the following relation:

$$\Delta T = \frac{RI^2}{L} \frac{1}{4\pi k} [\ln t + C^{te}] \quad (1)$$

where ΔT is the temperature gradient, R the resistance of the ring probe, k the thermal conductivity, I the current, t the pulse time, L the length of ring probe and C^{te} is the integration constant. The thermal conductivity and specific heat of carbon films are 0.762 W/mK and 1126 kJ/m³ K and 0.535 W/m K and 1256 kJ/m³ K for films deposited on FTO coated quartz and stainless steel substrates respectively. The high thermal conductivity on FTO coated quartz is mainly attributed to the significant change in microstructure. Apart from the contribution of the microstructure, the lower thermal conductivity of films can be attributed to the intrinsic factors. The thermal conductivity for a crystalline solid is due to changes of lattice vibrations, which are usually described in terms of phonons [34].

4. Conclusions

Influence of substrate on the structure and morphology of nanostructured carbon films by using thermal CVD have been investigated. XRD shows these films are crystalline with hexagonal and cubic: face-centered crystal structure for SS and FTO substrate respectively. Uniformly distributed carbon nanofibers have been detected for films on FTO glass. The contact angles of water droplets on the stainless steel and FTO coated surfaces are 134° and 114° respectively, which confirm the hydrophobic behaviour. FTIR reveals the C–H and O–H stretching vibrating modes corresponding to sp^3 and sp^2 carbon atoms. The presence of second-order bands in Raman spectra shows the formation of nanostructured growth of films.

Acknowledgement

One of the authors (S.S. Shinde) is highly grateful to the DRDO, New Delhi for the Senior Research Fellowship through its project ERIP/ER/0503504/M/01/007.

References

- [1] A.V. Melechko, V.I. Merkulov, T.E. McKnight, M.A. Guillorn, K.L. Klein, D.H. Lowndes, M.L. Simpson, *J. Appl. Phys.* 97 (2005) 041301.
- [2] S.S. Shinde, S.P. Patil, R.S. Gaikwad, R.S. Mane, B.N. Pawar, K.Y. Rajpure, *J. Alloys Compd.* 503 (2010) 416.
- [3] M. Tanemura, J. Tanaka, K. Itoh, T. Okita, L. Miao, S. Tanemura, S.P. Lau, L. Huang, Y. Agawa, M. Kitazawa, *Appl. Phys. Lett.* 87 (2005) 193102.
- [4] T.T. Tan, H.S. Sim, S.P. Lau, H.Y. Yang, M. Tanemura, J. Tanaka, *Appl. Phys. Lett.* 88 (2006) 103105.
- [5] U.B. Suryavanshi, C.H. Bhosale, *J. Alloys Compd.* 476 (2009) 697.
- [6] M. Tanemura, J. Tanaka, K. Itoh, Y. Fujimoto, Y. Agawa, L. Miao, S. Tanemura, *Appl. Phys. Lett.* 86 (2005) 113107.
- [7] M. Tanemura, M. Kitazawa, J. Tanaka, T. Okita, R. Ohta, L. Miao, S. Tanemura, *Jpn. J. Appl. Phys.* 45 (2006) 2004.
- [8] J. Song, M. Sun, Q. Chen, J. Wang, G. Zhang, Z. Xue, *J. Phys. D: Appl. Phys.* 37 (2004) 5.
- [9] N.S. Xu, Y. Chen, S.Z. Deng, J. Chen, X.C. Ma, E.G. Wang, *J. Phys. D: Appl. Phys.* 31 (2001) 1597.
- [10] G. Che, B.B. Lakshmi, E.R. Fisher, C.R. Martin, *Nature* 393 (1998) 347.
- [11] S. Wong, J.D. Harper, P.T. Lansbury, C.M. Lieber, *J. Am. Chem. Soc.* 120 (1998) 603.
- [12] J. Kong, R.N. Franklin, C. Zhou, M.G. Chapline, S. Peng, K. Cho, H. Dai, *Science* 287 (2000) 6226.
- [13] D.M. Guldi, G.M.A. Rahman, F. Zerbetto, M. Prato, *Acc. Chem. Res.* 38 (2005) 871.
- [14] A. Thess, R. Lee, P. Nikolaev, H. Dai, P. Petit, J. Robert, C. Xu, Y.H. Lee, S.G. Kim, A.G. Rinzler, D.T. Colbert, G.E. Scuseria, D. Tomanek, J.E. Fischer, R.E. Smalley, *Science* 273 (1996) 483.
- [15] C. Journet, W.K. Maser, P. Bernier, A. Loiseau, M.L. de la Chapelle, S. Lefrant, P. Deniard, R. Lee, J.E. Fisher, *Nature* 388 (1997) 756.
- [16] H. Dai, A.G. Rinzler, P. Nikolaev, A. Thess, D.T. Colbert, R.E. Smalley, *Chem. Phys. Lett.* 260 (1996) 471.
- [17] A.M. Cassell, J.A. Raymakers, J. Kong, H. Dai, *J. Phys. Chem. B* 103 (1999) 6484.
- [18] K. Mukhopadhyay, K.M. Krishna, M. Sharon, *Phys. Rev. Lett.* 72 (1994) 3184.

- [19] M. Sharon, K. Mukhopadhyay, K. Yase, S. Iijima, Y. Ando, X. Zhao, Carbon 56 (1998) 284.
- [20] C.R. Martin, Science 266 (1994) 1961.
- [21] G. Che, K.B. Jirage, E.R. Fisher, C.R. Martin, H. Yoneyama, J. Electrochem. Soc. 144 (1997) 4296.
- [22] C.M. Chen, Y.M. Dai, J.G. Huang, J.M. Jehng, Carbon 44 (2006) 1808.
- [23] S. Meier, et al., Surf. Coat. Technol. 202 (2007) 1267.
- [24] L. Vayssieres, Adv. Mater. 15 (2003) 464.
- [25] R.N. Wenzel, Ind. Eng. Chem. 28 (1936) 988.
- [26] K. Mukhopadhyay, M. Sharon, Mater. Chem. Phys. 49 (1997) 105.
- [27] Q. Wu, L. Yu, Y. Ma, Y. Liao, R. Fang, L. Zhang, X. Chen, K. Wang, J. Appl. Phys. 93 (2003) 94.
- [28] C. Ramaswamy, Nature 125 (1930) 704.
- [29] S.A. Solin, A.K. Ramdas, Phys. Rev. B 1 (1970) 1687.
- [30] J. Robertson, Adv. Phys. 35 (1986) 317.
- [31] S.S. Shinde, P.S. Shinde, V.G. Sathe, S.R. Barman, C.H. Bhosale, K.Y. Rajpure, J. Mol. Struct. (in press).
- [32] A.C. Ferrari, J. Robertson, Phys. Rev. B 61 (2000) 14095.
- [33] J.R. Shi, Diam. Relat. Mater. 10 (2001) 76.
- [34] S.S. Shinde, K.Y. Rajpure, J. Solid State Chem. (in press).